Heliyon 9 (2023) e16216

Contents lists available at ScienceDirect

Heliyon

journal homepage: www.cell.com/heliyon

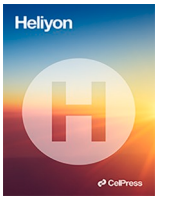

Research article

Room temperature sensing of primary alcohols via polyaniline/zirconium disulphide

Paul Fadojutimi [a,*], Clinton Masemola [a], Manoko Maubane-Nkadimeng [b], Ella Linganiso [b], Zikhona Tetana [b], John Moma [a], Nosipho Moloto [a], Siziwe Gqoba [a,**]

[a] Molecular Sciences Institute, School of Chemistry, University of the Witwatersrand, Johannesburg, 2050, South Africa
[b] Microscopy and Microanalysis Unit, University of the Witwatersrand, Johannesburg, 2050, South Africa

ARTICLE INFO

Keywords:
Response
Room temperature
Polyaniline
Polyaniline-zirconium disulphide

ABSTRACT

Among the primary alcohols, ethanol is referred to as a heavy chemical due to its many applications in a variety of industries. Detection of primary alcohols can be deployed as a non-invasive method in medical diagnosis and safety measures in food processing companies. Zirconium disulphide is a novel 2D layered material with exotic features when in mono or few layers, which include fast electron transport, high carrier mobility and sizeable band gap. ZrS_2 and PANI were fabricated using liquid exfoliation and chemical polymerization methods respectively. Functionalization of the conducting polyaniline with ZrS_2 was done using facile sonication process. The sensor showed good sensitivities (43%, 58% and 104%) which were estimated from slopes of the linear fitted plots with fast response-recovery times of 8 s and 27 s (111 ppm); 12 s and 130 s (77 ppm); and 58 s and 88 s (58 ppm). Good reproducibility at three repeated measurements (111 ppm, 77 ppm and 58 ppm) was also observed for methanol, ethanol, and isopropanol vapours respectively. Meanwhile, the sensor displayed more linearity and sensitivity towards isopropanol compared to methanol and ethanol. The sensor showed good performance even at RH values close to 100% making it a potential alcohol breath analyser.

1. Introduction

It is about sixteen decades now ever since the existence of polyaniline (PANI); however, its conductive nature was only discovered just four decades ago. Polyaniline as a conducting organic polymer has found a great application in sensors (chemical and biological) due to its ease of production, environmental stability, and reversible redox chemistry [1,2]. PANI is commonly fabricated using two methods: electrochemical polymerization and chemical polymerization. Moreover, the chemical polymerization method is commonly deployed in gas sensing applications since it can be easily tailored to fabricate nanostructures and various morphologies compared to the other methods.

1D dimensional PANI such as nanofibers, nanowires and nanorods are the mostly fabricated morphologies using aniline (monomer) and ammonium persulphate (APS) which plays the role of an oxidant in acidic media. The protonation of the polyaniline is very essential; this is the means in which PANI turns out to be electrically conductive. PANI is utilized in chemical sensing to serve as a replacement for metal oxide semiconducting nanomaterials. It offers the advantages of low cost, ease of fabrication, tunable

* Corresponding author.
** Corresponding author.
E-mail addresses: paulfadthechemist@yahoo.com, Paul.Fadojutimi@wits.ac.za (P. Fadojutimi), Siziwe.Gqoba@wits.ac.za (S. Gqoba).

https://doi.org/10.1016/j.heliyon.2023.e16216
Received 23 February 2023; Received in revised form 4 May 2023; Accepted 10 May 2023
Available online 12 May 2023

conductivity, high porosity, and sensitivity at room temperature (RT). However, PANI based sensors have few demerits such as poor response time, poor selectivity, low reproducibility, and poor stability. To counter these drawbacks, nanocomposites of polyaniline with 2D materials, carbon materials and metals have been used and they reportedly improved the response time and stability of PANI based sensors. Hence, proffering a solution to these demerits is very essential by using novel nanomaterials with proper attributes for chemical sensing [1,2].

Functionalization of PANI with transition metal dichalcogenides (TMDCs) to enhance the sensor attributes arising from synergetic effects has been reported in literature. More research has been reported on group VI TMDCs compared to groups V and IV TMDCs. Generally, few published works are available on group IV TMDCs despite theoretical findings showing these nanomaterials as possessing astonishing properties. For instance, in relation to chemical sensing application, it was speculated that TiS_2 has more active sites for gas absorption than MoS_2 owing to crystal structure and bonding that exist between the metal and the sulphur atoms [3]. It was also predicted that monolayer ZrS_2 will be suitable for gas sensing. The author also reported that a defect ZrS_2 with *S*-vacancies will behave as a better sensor compared to ZrS_2 with no defect [4]. Few works were reported on pristine TiS_2, and its nanocomposite with conducting polymers in literature for chemical sensing, therefore more extensive research is very paramount. In terms of sensor, ZrS_2 has only been demonstrated as an optical coupled plasmon waveguide resonance (CPWR) sensor but not as a chemiresistive sensor [5].

ZrS_2 is a novel 2D layered material with exotic features when in mono or few layers, which include fast electron transport, high carrier mobility and sizeable band gap. The material is environmentally friendly, has good thermodynamic stability, very abundant in the earth's crust unlike rare earth metals which are not cost effective and very limited in nature [4,6]. There are weak van der Waals forces that exist in between the layers and covalent bonds within the material. It also possesses outstanding electronic properties and a large specific surface area owing to high surface to volume-ratio. ZrS_2 nanomaterials is highly sought after due to its application in solar cells, field effect transistors (FETs), thermoelectric devices, photo detectors, fiber lasers, optics, sensors, tribology, electode materials and catalysis [7]. Kishoro et al. was the first to report on chemical sensing of group IVB TMDCs in which TiS_2 was demonstrated for the sensing of O_2 and N_2 at a temperature of 50 °C. The sensor displayed a short response time but a very slow recovery time [8]. Shokouh et al. reported a fascinating recovery with an ultra-fast time of 2 s and response time of 60 s for ethanol sensing by a nanohybrid of TiS_2 and polyvinyl polymer (PVP) [3]. However, though a fast recovery time was achieved which is a great improvement for TMDCSs sensor but the response time of 1 min still needed to be improved. Manjunata et al. reported on the good sensitivity, rapid response time and recovery time demonstrated by nanohybrid of tantalum disulphide and polyaniline (PANI/TaS_2) for humidity sensing [9]. Sakhuja et al. investigated TiS_2 nanosheets towards H_2S and O_2 at room temperature. The sensor showed high sensitivity of 111.8%, quick response-recovery times of 19.7 and 48 s respectively towards 4 ppm of H_2S [10]. Shaukat et al. recently reported on $ZrSe_2$ towards humidity with a range of 15–80% RH. The sensor displayed good sensitivity of 68 KΩ, fast response-recovery times, good reproducibility, and good stability [11]. Recently, Sharma et al. observed response and recovery times of 72 and 175 s respectively at room temperature by TiS_2 sheets toward ammonia vapour [12]. Extensive investigation has been undertaken on NH_3 and NO_2 vapour sensing based on TMDC sensors such as MoS_2, $MoSe_2$, WS_2, WSe_2, SnS_2 and $SnSe_2$, however, very few reports are available on alcohols and acetone vapour sensing [13–18]. There is still much to be investigated on group IVB TMDCs on sensing of VOCs especially alcohols. Shokouh et al. only reported on ethanol vapour, while the reproducibility and linear response of the sensor were not mentioned [3].

This current work demonstrates the fabrication of a low-cost sensor of zirconium disulphide and polyaniline nanocomposite, and its application for sensing chemical vapours at RT for the first time. The sensor demonstrates good linearity, quick sensitivity, fast response-recovery times, and reproducibility towards alcohol vapours.

1.1. Chemicals and materials

Zirconium disulphide [99%, ZrS_2, C.C. Imelmann (pty) ltd], isopropyl alcohol [99%, IPA, MK Chemicals], ammonium persulphate [99.9%, APS, Sigma-Aldrich], aniline [99.9%, Sigma-Aldrich] HCl 32% [Associated chemical enterprises] were used as received without further purification. A mortar and pestle, a PS-20A sonicator bath with a power of 100 W.

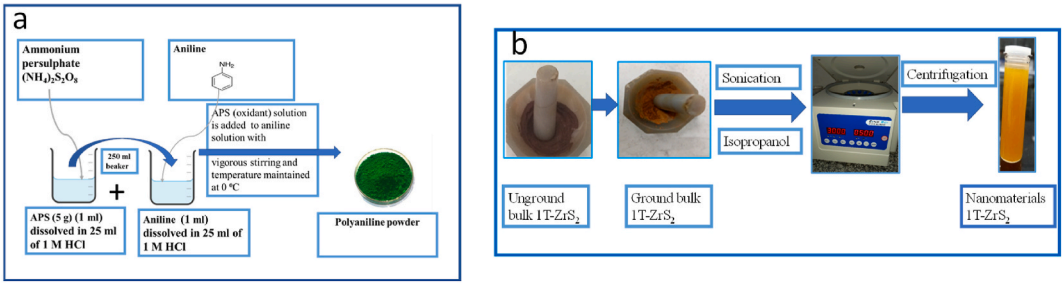

Fig. 1. (a) Schematic diagram depicting the synthesis of PANI. (b) Exfoliation of bulk crystal of zirconium disulphide.

2. Methods

2.1. Synthesis of PANI

The method described by Masemola et al. was used for the synthesis. In a typical synthesis, as shown in Fig. 1(a), 1.50 g of ammonium persulphate (APS) and 1 mL of aniline were dissolved in two separate 250 mL beakers containing 25 mL of HCl [19]. The aqueous solution of APS was slowly transferred into the second beaker containing aniline with constant stirring of the solution and reaction maintained at about 0 °C. This is very essential as the reaction is very exothermic, it may lead to decomposition of the polyaniline polymer formed. After a few minutes, the reaction went to completion and the green PANI precipitate was obtained by filtration. PANI was then washed with a solution of 1 M HCl to remove any unreacted aniline followed by multiple washing with distilled water. Finally, the polymer was dried in an oven at a temperature of 40 °C.

Exfoliation of ZrS_2

The method of synthesis was adopted from Li et al. the bulk sample of about 1.00 g was ground for about 2 h and 5.00 mg of the sample was transferred to a vial. A volume of 12 mL of IPA was introduced and the vial was covered and wrapped with parafilm. The solution was then transferred to a bath sonicator and sonicated for 24 h [20]. The temperature was maintained at about 25 °C by introducing ice cubes into the bath sonicator at regular intervals. The set-up of the reaction is shown in Fig. 1(b). After exfoliation, the resulting solution was centrifuged at 2000 rpm for 30 min to separate the exfoliated from the unexfoliated sample. The supernatant was collected and centrifuged for 15 min at 1500 rpm. The low speed of centrifugation is needed to effectively separate the exfoliated and non-exfoliated nanomaterials. From the inset in Fig. 1(b), it can be observed that the bulk sample was pecan brown before grinding and the colour changed to light brown during grinding in ambient environment; this may be ascribed to possible slight oxidation of the sample. The exfoliated nanosheets of ZrS_2 dispersion in IPA produced a homogeneous solution with good dispersion of yellow colouration.

PANI and ZrS_2 (PANI-ZrS_2) nanocomposite.

A nanocomposite of PANI and zirconium disulphide was fabricated by introducing 5.00 mg of ZrS_2 into a vial containing 95.00 mg of polyaniline in IPA; the vial was sealed and wrapped with parafilm. The vial was sonicated for 24 h after which the resulting solution was filtered, and the product dried at room temperature.

Sensor fabrication.

The PANI-ZrS_2 based sensor was prepared on a printed circuit board (PCB) FR4 substrate. Interdigitated electrodes were patterned on the rectangular shaped PCB consisting of electroless nickel immersion gold electrodes of 18 pairs with a length of 7.9 mm and a space of 0.1 mm between each electrode. The sensing film was prepared by drop casting 15 μL of the film that was prepared by sonicating 5.00 mg of nanocomposite of PANI-ZrS_2 in 500 μL of methanol for 10 min.

Gas sensing measurements.

All electrical measurements were conducted at RT. An LCR-6300 10 Hz−300 KHz precision LCR meter coupled to a computer. The frequency and voltage were set at 10 KHz and 1.00 V respectively. The system was allowed to stand for a few minutes before any measurements were done. The set-up for gas sensing is shown in Fig. 2 below.

The vapour sensing experiment was conducted at RT; the response values were recorded using a data logger (LCR). The vapour

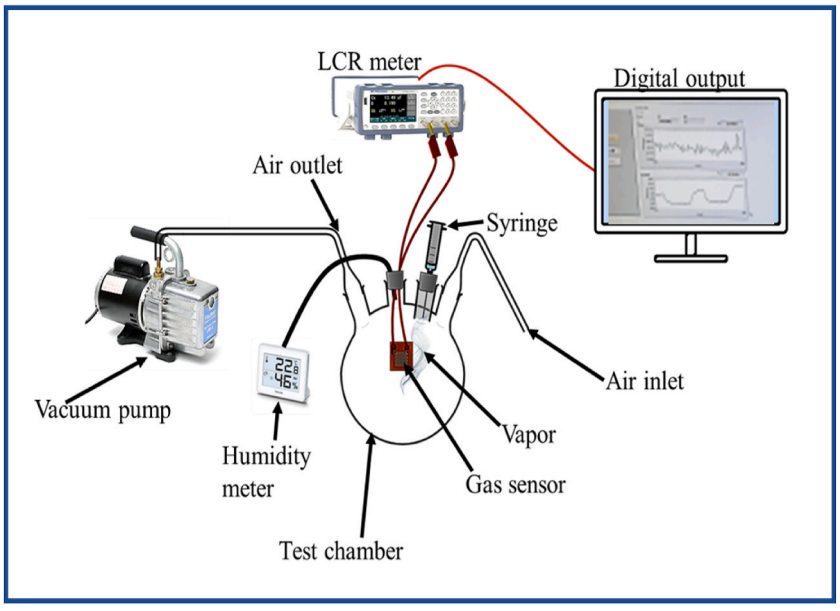

Fig. 2. Schematic diagram of the gas sensing set-up.

sensing properties were explored by injecting a measured volume of anhydrous alcohol (methanol) into a closed glass chamber (5 L) via a glass syringe. The concentration of the methanol vapour in the test chamber can be evaluated in ppm by using the following equation:

$$C = \frac{224\rho TVs}{273MV} \text{ x}100 \quad (1)$$

here C represents concentration of methanol vapour (ppm), ρ is the density of the solvent (gML^{-1}), T is the temperature in Kelvin, Vs is the volume of the solvent, M is the molecular weight of the solvent. The following concentrations were obtained 111, 222, 333, 444 and 555 ppm which correspond to 1–5 μL injections with the syringe. The response of the sensor is obtained as $S = (R_a\text{-}R_g)/R_a \times 100$, where Ra and R_g represented resistance in air and methanol vapour respectively. The duration involved by a sensor to complete 90% of the resistance change is known as response/recovery time. The sensor measurements were also conducted for ethanol and isopropanol vapour. The sensor was exposed to methanol vapour at various concentrations. To ensure the vapour reaches saturation point upon injection of the gas, the sensor was allowed to interact with the analyte gas for 300 s for proper adsorption and 200 s for the desorption of the vapour (recovery). The same procedure was conducted for ethanol and isopropanol.

2.2. Characterization

Powder X-ray diffraction (PXRD) analysis was performed using a Bruker D2 phaser (D2-205530) diffractometer with Cu Kα1 radiation (λ = 1.54060 Å) at 30 kV and 10 mA. Transmission electron microscopy (TEM) (Jeol JEM-2100F 200 kV) was used to analyse the morphology of the a-synthesized PANI and nanocomposite of PANI-ZrS_2. The surface area and porosity were measured using Micromeritics RS232 and porosity analyzer instrument. The surface area measurements were performed via N_2 adsorption/desorption and calculated by the Brunauer Emmett and Teller (BET) analysis method.

3. Results and discussion

3.1. XRD analysis

Fig. 3 shows the XRD crystallographic structure of the PANI-ZrS_2 nanocomposite. Fig. 3(a) shows the XRD pattern of PANI with only one peak as shown with diffraction peak at 20.32° which corresponds to (020) crystal plane of PANI in its emeraldine salt form [21]. Fig. 3(b) shows the ZrS_2 pattern matches hexagonal ZrS_2 indexed to JCPDS card of 010605262. The following diffraction peaks: 15.45, 28.57, 32.34, 42.10, 50.25, 55.8 and 60.94° which correspond to the (001), (100), (101), (102), (110), (103), and (201) planes of ZrS_2 were identified. However, as seen in Fig. 3(c) the nanocomposite peaks seem more crystalline than unmodified ZrS_2 and pristine PANI. In addition, more peaks were observed at about 25.56, 46.25 and 52.68 which correspond to crystal planes of ZrS_2 at (003), (111) and (202) while the peak at 67.58° correspond to PANI at (200) in its emeraldine salt form. The diffraction peak at about 35.20 is ascribed to the oxide of zirconium due to possible oxidation of ZrS_2 in ambient environment and diffraction peaks at about 28.40 and 44.00° are ascribed to peaks of ZrS_3 which is most likely formed during formation of ZrS_2 by chemical vapour transport [7,22].

3.1.1. TEM analysis

The TEM micrographs show the morphologies of the pristine PANI, untreated ZrS_2 and PANI-ZrS_2 nanocomposite. The pristine

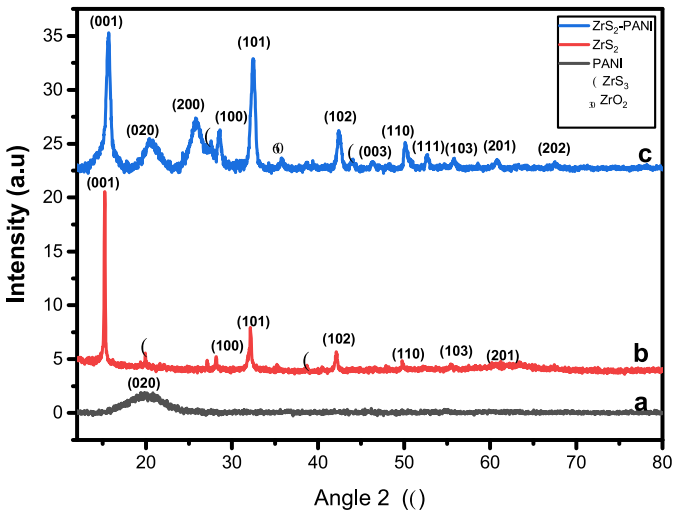

Fig. 3. (a) XRD pattern of PANI. (b) XRD pattern of ZrS_2 and (c) XRD pattern of PANI-ZrS_2 nanocomposite.

PANI and untreated ZrS_2 as well as its nanocomposite all exist in layers of nanosheets as shown in Figs. 4(a,b) and 5(a–d), so it is quite difficult to distinguish between the two nanosheets, however, the dark stains represent nanosheets of ZrS_2 in PANI nanosheets. Several authors have reported on 1D PANI for different applications such as gas sensing and supercapacitors compared to 2D dimensional PANI.

3.1.2. BET analysis

Figs. 6(a) and 7(a) show nitrogen adsorption-desorption isotherms of PANI-ZrS_2 and PANI respectively; and 6(b) and 7(b) show pore-size distributions of PANI-ZrS_2 and PANI respectively. A steady increase in the volume of N_2 absorbed and desorbed can be noticed at about relative pressure of 0.82–0.98 nm for the nanocomposite of PANI-ZrS_2 and pristine PANI, these represent type IV isotherm [23]. The surface area of PANI increased from 27.87 m^2/g to 28.95 m^2/g with the nanocomposite and Barrett Joyner-Halenda (BJH) method was used to determine pore size distribution (PSD), the pore size increased from 0.18 to 0.19. These show that the nanocomposite is microporous as well as pristine PANI. The improvement in the surface area and small pore size of the PANI-ZrS_2, shows it contain a plethora absorption sites to improve the interactions that exist with volatile organic molecules and the sensor.

3.1.3. Gas sensing by PANI-ZrS_2 nanocomposite

TMDCs and PANI sensors generally can sense chemical/gas vapours at room temperature, this gives them an advantage over metal oxide sensors that often require temperature that exceed RT [24]. Operating a sensor at elevated temperature may lead to structural changes in the sensing material whose effects are instability and response disparity. PANI is an n-type chemiresistive sensor. PANI chains are made up of two structural units; a reduced [B–NH–B–NH] and oxidized [B–N = Q = N] repeating units, where B and Q represent benzenoid and quinoid rings respectively. Swelling of PANI is likely possible being a polymer with a rigid backbone. When a reducing chemical vapour such as alcohols is introduced to a PANI sensor, the reducing chemical donates an electron to the polymer matrix, which leads to an increase in the resistance of the sensor due to change in the concentration of the sensing material holes. Whereas when oxidizing gases like NH_3, NO_2, H_2S and I_2 are injected, deprotonation of PANI occurs hence, the increase in resistance of the sensor. On exposure of the sensor to dry air, the opposite mechanism which is protonation of PANI occurs [25,26]. There is change in conductance upon an increase in vapour concentration. PANI and its substituted derivatives have been reported to be sensitive to first to fourth members of primary alcohols and heptanol vapours. Small chain alcohol result into a decrease in electrical resistance, however the reverse is the case with long chain alcohol. With ethanol, the doping or oxidation state remains the same and hence has negligible impact on the conductivity of PANI. Swelling of PANI backbones is very possible with ethanol therefore, there is an increase in the electrical resistance of the sensor. Fig. 8 shows the schematic representation of the sensing mechanism of PANI-ZrS_2 to ethanol vapour. Incorporating ZrS_2 with PANI provides a synergistic effect by improving the features of PANI sensor and enhancing the sensitivity of the sensor or boost its selectivity or both. ZrS_2 nanosheets integration with PANI, forms n-p heterojunction with a depletion layer. A change in depletion region will take place upon adsorption of gases by the nanocomposite [26].

Primary alcohol sensing properties.

Fig. 9 (a) depicts a static response curve of methanol vapour at room temperature in 45% RH to 111 ppm of methanol. A good signal with relatively weak noise to methanol vapour can be deduced from the response curve. It took about 400 s for the sensor to attain saturation time upon exposure to the analyte. A total recovery of the sensor on exposure to air is also noticed. Two adsorption stages were observed towards methanol vapour at 111 ppm. The response and recovery times were extrapolated from the graph to be 8 s and 27 s respectively.

Fig. 10 (a) shows the dynamic response curves of PANI and PANI-ZrS_2 sensors toward methanol vapour at different concentrations (111–555 ppm) at room temperature (RT) in 47% RH with exposure time of 300 s in vapour and 200 s in air.

Fig. 10 (b) shows response curves of the nanocomposite measured at different methanol concentrations (111–444 ppm). Measurements were conducted from low vapour concentration to high vapour concentration and vice versa. Both PANI and PANI-ZrS_2 sensors show a rise in response with increase in vapour concentration as seen in Fig. 10 (a). The PANI-ZrS_2 sensor showed significant improvement compared to the PANI sensor response up to 9 folds due to the close interface that existed between the PANI and ZrS_2. The enhanced response is due to synergistic effect.

Fig. S1 displayed the repeatability nature of the PANI-ZrS_2 film sensor to 111 ppm methanol vapour at RT with three repetitive response-recovery curves. The sensor showed a clear response-recovery output and stable three repetitive response-recovery curves for

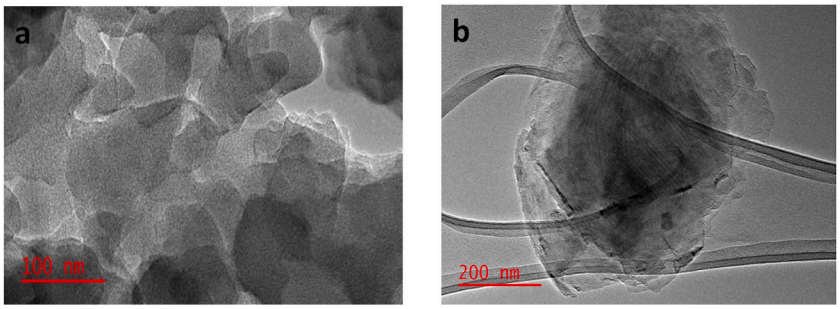

Fig. 4. (a) TEM image of PANI. (b) TEM image of ZrS_2 nanosheets.

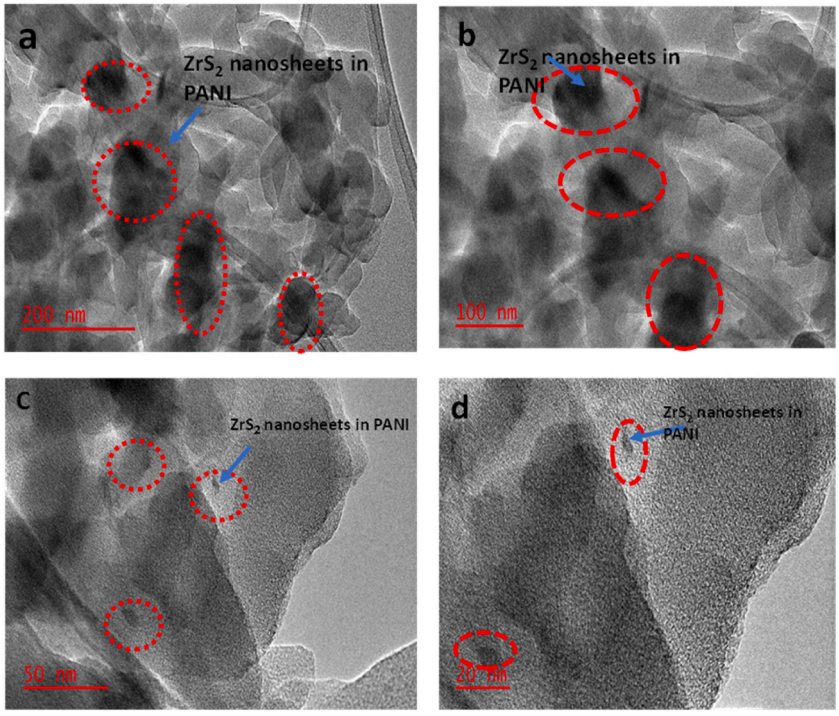

Fig. 5. (a) TEM image of PANI-ZrS_2 nanocomposite at 200 nm. (b) TEM image of PANI-ZrS_2 nanocomposite at 100 nm. (c) TEM image of PANI-ZrS_2 nanocomposite at 50 nm. (d) TEM image of PANI-ZrS_2 nanocomposite at 20 nm.

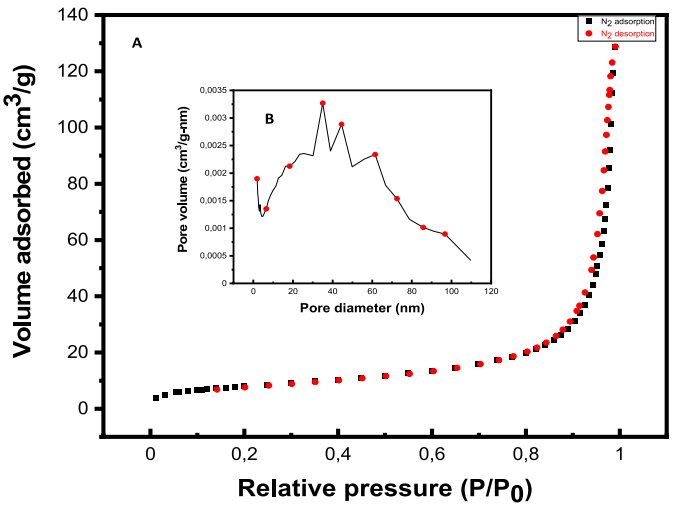

Fig. 6. (a) Nitrogen adsorption-desorption isotherm for PANI-ZrS_2. (b) BJH pore size distributions of PANI-ZrS_2.

methanol vapour sensing.

The time-dependent response and recovery curves of PANI-ZrS_2 to ethanol at 77 ppm and 385 ppm is depicted by Fig. 11(a). The sensor response to 77 ppm ethanol vapour had a longer saturation time (>600 s) while 385 ppm vapour concentration had a lesser saturation time (<600 s). The sensor displayed a two - stage adsorption towards ethanol vapour which is shown by a rapid adsorption within the 180 s: thereafter a moderate adsorption at about saturation time of 600 s. This may be ascribed to possible defects of ZrS_2 or PANI or both resulting to differing affinity for ethanol vapour by the sensor giving rise to incremental saturation. Similar observation was reported by Mutuma et al. where untreated hollow carbon spheres resulted in two adsorption stages towards ammonia vapour [27]. The response and recovery times were extrapolated from the graph to be 83 s and 44 s respectively to 385 ppm of ethanol vapour.

Fig. 11(b) depicts dynamic response curves of PANI and PANI-ZrS_2 sensors toward ethanol vapour at varying concentrations (77–385 ppm) at RT in 45% RH with exposure time of 300 s and 200 s in gas and air respectively. Both sensors produced an increase in

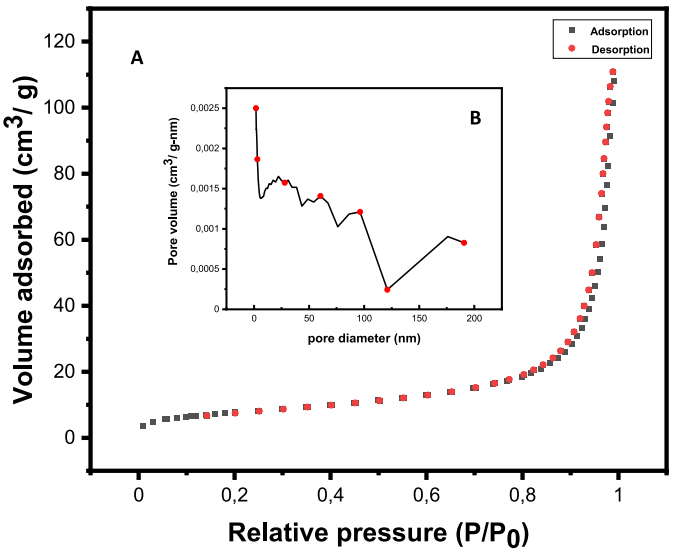

Fig. 7. (a) Nitrogen adsorption-desorption isotherm for PANI. (b) BJH pore size distributions of PANI.

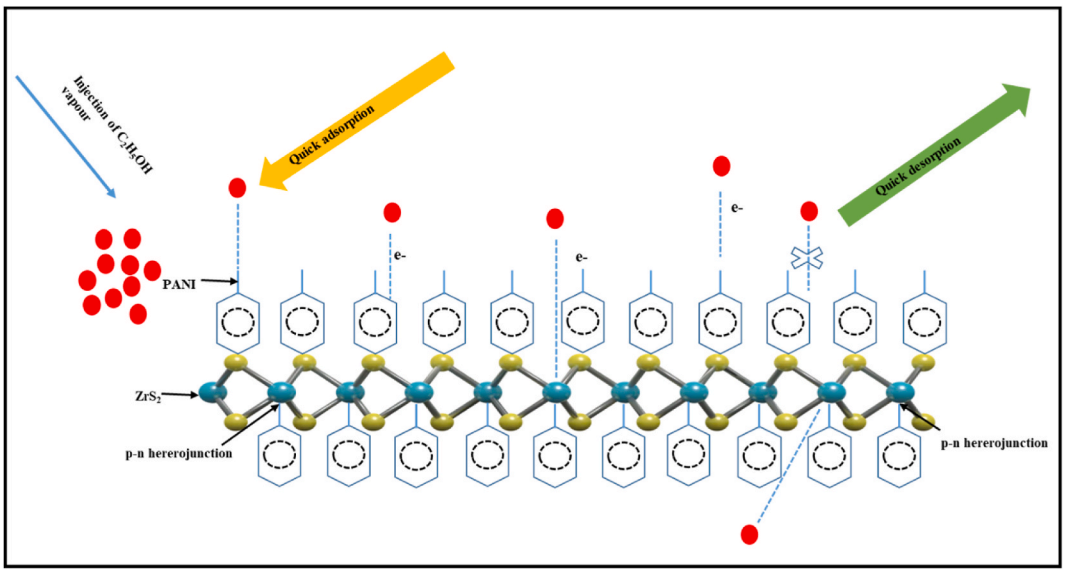

Fig. 8. Schematic illustration of sensing mechanism of PANI-ZrS_2.

response with increase in vapour concentration introduced. The PANI-ZrS_2 nanocomposite amplified the performance of the sensor to ethanol vapour sensing characteristics in comparison to pristine PANI.

The reproducibility of a sensor is a very paramount factor, as this determines the reliability of the chemical sensor for practical purposes. Fig. S2 depicts the reproducibility nature of the PANI-ZrS_2 film sensor to 77 ppm ethanol vapour at RT with three repetitive response-recovery curves. The sensor demonstrated a clear response-recovery output and stable three repetitive response-recovery curves for ethanol vapour sensing.

Fig. 12 (a) depicts a static response curve of isopropanol vapour at room temperature in 45% RH to 58 ppm of isopropanol vapour. A good signal with relatively weak noise to isopropanol vapour can be obtained from the response curve. It took about 675 s for the sensor to attain saturation time upon exposure to the analyte. A total recovery of the sensor on exposure to air is also noticed, the response and recovery times were extrapolated from the graph to be 58 s and 88 s respectively.

Fig. 12(b) depicts the dynamic response curves of PANI and PANI-ZrS_2 sensors towards isopropanol vapour at distinct concentrations (58–289 ppm) at RT in 45% RH with exposure time of 300 s in gas and 200 s in air.

Fig. S3 depicts the reproducibility of the sensor to 58 ppm isopropanol vapour at RT with three repetitive response-recovery curves. The sensor demonstrated a clear response-recovery output and stable three repetitive response-recovery curves for isopropanol vapour

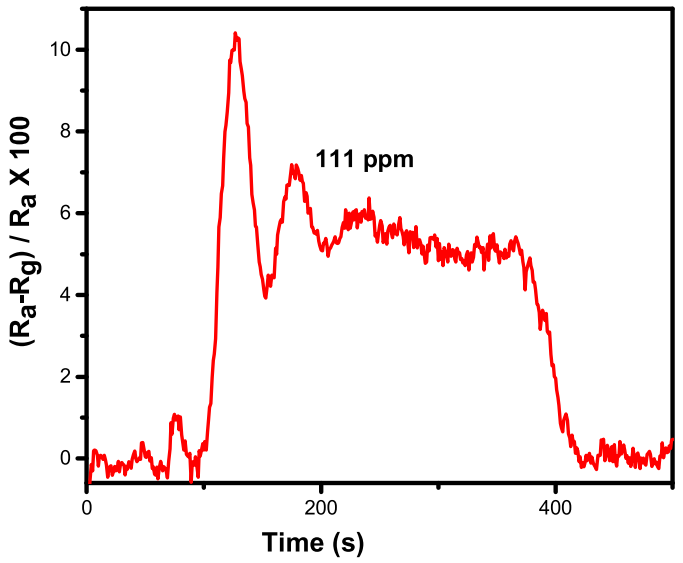

Fig. 9. Static response of PANI-ZrS_2 towards methanol vapour at RT.

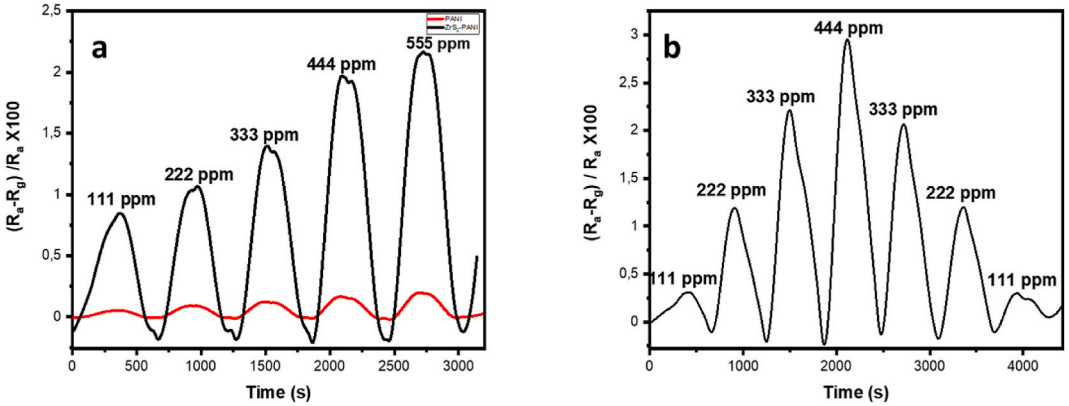

Fig. 10. (a) Dynamic response curves of PANI-ZrS_2 towards methanol vapour at RT (b) Response curves of the PANI-ZrS_2 sensor taken under various methanol vapour concentration.

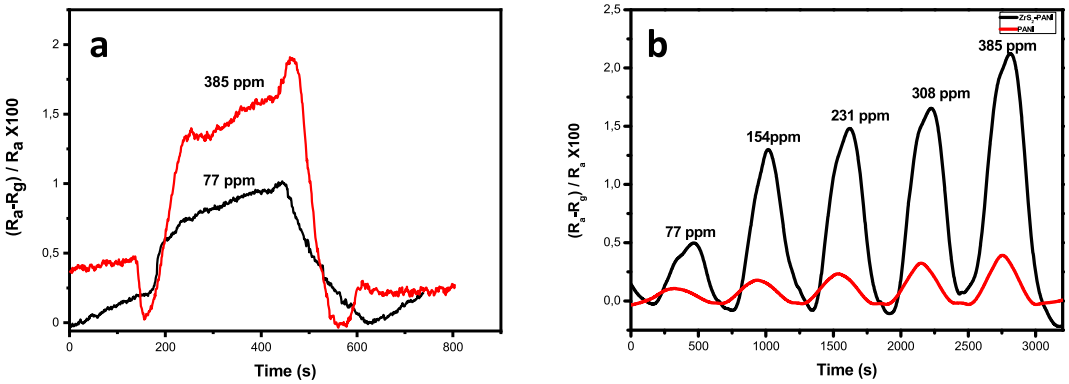

Fig. 11. (a)Typical response and recovery curves of PANI-ZrS_2 sensor to ethanol at 77 ppm and 385 ppm respectively. (b) Dynamic response and recovery curves of PANI-ZrS_2 towards ethanol vapour at RT.

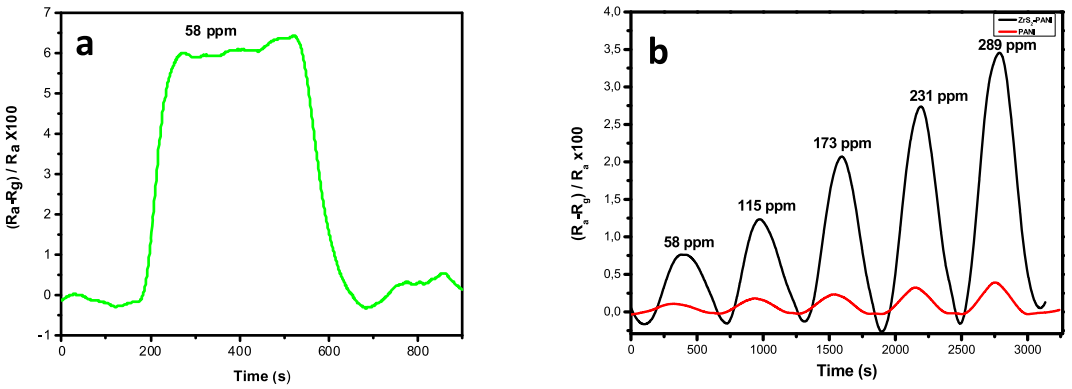

Fig. 12. (a) Static response and recovery curves of PANI-ZrS_2 sensor to isopropanol vapour at RT. (b) Dynamic response and recovery curves of PANI-ZrS_2 towards isopropanol vapour at RT.

sensing.

Fig. 13 (a) shows the sensitivity of the PANI-ZrS_2 sensor to different alcohol vapours. The sensitivity was extrapolated from their linear fitted plots (Fig. 13(b)). The response of the sensor to isopropanol is about a multiple of two compared to ethanol and had least sensitivity to methanol vapour. This is may be ascribed to the difference in their binding energy to the sensor [18]. The sensitivity to methanol, ethanol and isopropanol was calculated from the slope of their linear fitted graphs in Fig. 13(b) as 43%, 58% and 104% respectively. Functionalization of PANI with ZrS_2 could be a good promoter for development of sensors with an enhanced performance at room temperature.

Table 1 shows the performance of PANI-ZrS_2 sensor compared to other TMDCs and their nanocomposite for VOCs sensing and RH with good sensitivity and rapid response time while pure ZrS_2 in this work manifested poor conductivity and has resulted in no response to VOCs at room temperature. This may be due to fact that the ZrS_2 nanosheets used in this work have many layers.

3.1.4. Relative humidity

Relative humidity is another important factor which can affect the performance of a sensor, it either causes a rise or decline in response. This factor normally affects sensors at RT. The relative humidity of the sensor was conducted for methanol and ethanol vapours at RT as shown in Fig. 14 (a) and (b). The effect of humidity on methanol sensor was maximum at 64%; while for ethanol vapour at a pronounced humidity of 75% the sensor behaviour changed from p-type to n-type and maximum response was observed at 96%. Factors such as type of analyte, temperature, humidity affects the behaviour of a sensor.

4. Conclusion

Group IVB TMDCs have exotic properties, which make them suitable for chemical sensing. The nanocomposite demonstrated good sensing of primary alcohols at RT. The sensor displayed more sensitivity towards isopropanol compared to methanol and ethanol. The behaviour of the sensor changed from p-type to n-type on exposure to ethanol vapour at elevated relative humidity. The sensor also showed good response to low concentrations (7.7 ppm, 11 ppm, 5.8 ppm) which correspond to methanol, and ethanol, isopropanol respectively. The sensor may find application in industrial and medical purposes. The sensor displayed good sensitivity, reproducibility, rapid response, and recovery times towards alcohols. The sensitivity and selectivity of the sensor may be improved at room

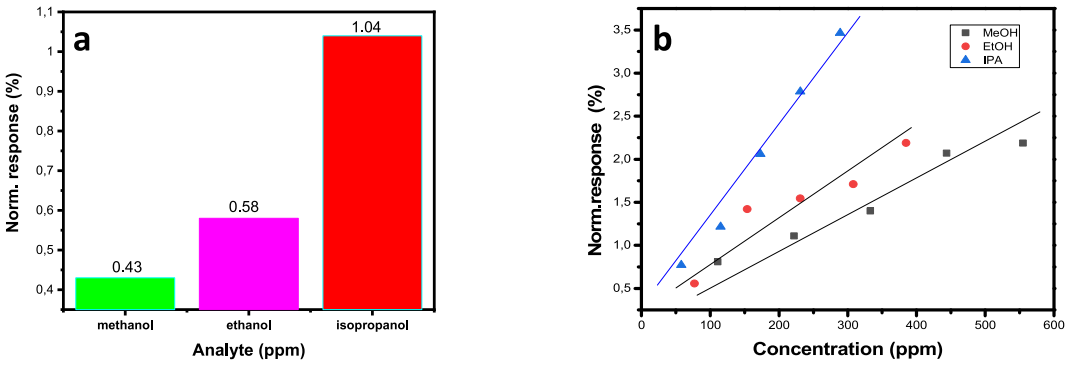

Fig. 13. (a) Comparison of PANI-ZrS_2 sensor towards methanol, ethanol, and isopropanol vapour at RT. (b) Normalized response of the PANI-ZrS_2 sensor towards methanol, ethanol, and isopropanol.

Table 1
Group IVB TMDCs and TMDCs nanocomposite with polymers for VOCs and RH sensing.

T °C	Gas (ppm)	Sensitivity (%)	Response time (s)	Recovery time (s)	References
RT	H_2O	97	36	49	[8]
RT	NH_3	75.6	–	–	[28]<
RT	C_2H_5OH (2)	6800	60	2	[3]
RT	H_2S (4)	111.8	19.75	48	[10]
RT	H_2O	–	–	–	[11]
RT	NH_3		72	175	[12]
RT	C_2H_5OH (385)	52	83	44	This work
	CH_3OH (555)	43	78	69	
	C_3H_7OH (58)	104	44	88	

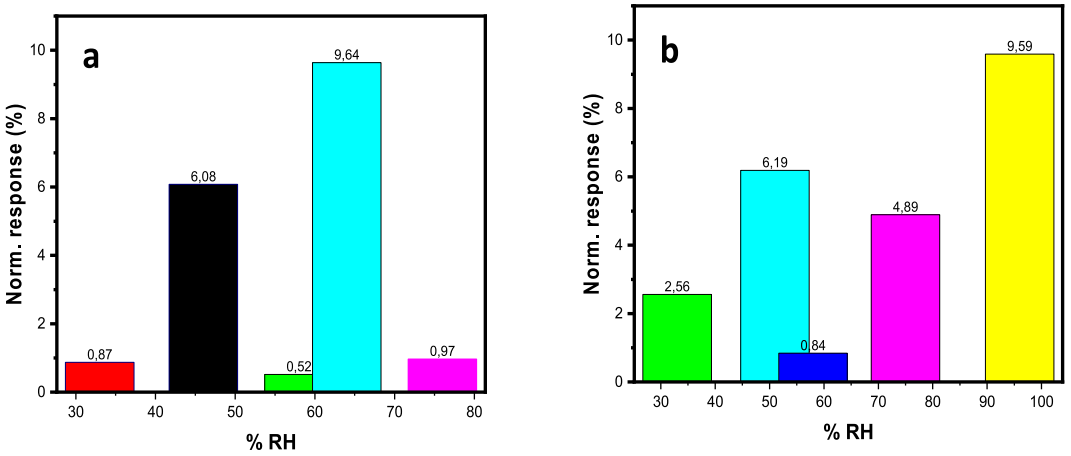

Fig. 14. Response of PANI-ZrS_2 towards (a) 111 ppm of methanol vapour; (b) 77 ppm of ethanol vapour under different humidity conditions at 33, 46,58, 64 and 76% for methanol and at 33, 51, 58, 75 and 96% for ethanol.

temperature by electrospinning of PANI-ZrS_2 nanocomposite to produce nanofibers of high specific surface area.

Author contribution statement

Paul Olawale Fadojutimi: Performed the experiments; Analyzed and interpreted the data; Wrote the paper.
Clinton Micheal Masemola: Analyzed and interpreted the data.
Manoko Maubane-Nkadimeng, Ella Linganiso: Analyzed and interpreted the data; Contributed reagents, materials, analysis tools or data.
Zikhona Tetana, John Moma: Conceived and designed the experiments; Contributed reagents, materials, analysis tools or data.
Nosipho Moloto, Siziwe Gqoba: Conceived and designed the experiments; Analyzed and interpreted the data; Contributed reagents, materials, analysis tools or data.

Data availability statement

Data will be made available on request.

Declaration of competing interest

The authors declare no conflict of interest.

Acknowledgements

Many thanks to Wits University URC for funding this research work.

Appendix A. Supplementary data

Supplementary data to this article can be found online at https://doi.org/10.1016/j.heliyon.2023.e16216.

References

[1] E. Song, J.W. Choi, Conducting polyaniline nanowire and its applications in chemiresistive sensing, Nanomaterials 3 (3) (2013) 498–523.
[2] A. Sayah, F. Habelhames, A. Bahloul, et al., Electrochemical synthesis of polyaniline-exfoliated graphene composite films and their capacitance properties, J. Electroanal. Chem. 818 (April 2017) (2018) 26–34.
[3] S.H. Hosseini-Shokouh, S. Fardindoost, A.I. Zad, A high-performance and low-cost ethanol vapor sensor based on a TiS_2/PVP composite, ChemistrySelect 4 (21) (2019) 6662–6666.
[4] H.T.T. Nguyen, D.Q. Hoang, T.P. Dao, et al., The characteristics of defective ZrS2 monolayers adsorbed various gases on S-vacancies: a first-principles study, February, Superlattice. Microst. 140 (2020) (2020), 106454.
[5] J.M.A. Inying, L.U. Kunl, J.U.J. Iang, et al., All optic-fiber coupled plasmon waveguide resonance sensor using ZrS2 based dielectric layer, Optics Exp. 28 (8) (2020) 11280–11289.
[6] Y. Shimazu, Y. Fujisawa, K. Arai, T. Iwabuchi, K. Suzuki, Synthesis and characterization of zirconium disulfide single crystals and thin-film transistors based on multilayer zirconium disulfide flakes, ChemNanoMat 4 (10) (2018) 1078–1082.
[7] P.O. Fadojutimi, S.S. Gqoba, Z.N. Tetana, J. Moma, Transition metal dichalcogenides [MX2] in photocatalytic water splitting, Catalysts 12 (2022) 468.
[8] K. Kishiro, S. Takemoto, H. Kuriyaki, K. Hirakawa, Resistivity response to oxygen of transition metal dichalcogenide TiS2, Jpn. J Appl. Phys. 1 Regul. Pap. Short Notes Rev. Pap. 33 (2) (1994) 1069–1073.
[9] S. Manjunatha, T. Machappa, Y.T. Ravikiran, B. Chethan, A. Sunilkumar, Polyaniline based stable humidity sensor operable at room temperature, Phys. B Condens. Matter 561 (March) (2019) 70–178.
[10] N. Sakhuja, R.K. Jha, R. Chaurasiya, A. Dixit, N. Bhat, 1T-Phase titanium disulfide nanosheets for sensing H_2S and O_2, ACS Appl. Nano Mater. 3 (4) (2020) 3382–3394.
[11] R.A. Shaukat, M.U. Khan, Q.M. Saqib, et al., Two dimensional Zirconium Diselenide based humidity sensor for flexible electronics, Sensor. Actuator. B Chem. 358 (February) (2022), 131507.
[12] S. Sharma, S. Singh, R.C. Singh, S. Sharma, Structural transformation and room temperature ammonia sensing properties of TiS_2 nanostructures, SN Appl. Sci. 2 (5) (2020) 1–12.
[13] D.J. Late, Y.K. Huang, B. Liu, et al., Sensing behavior of atomically thin-layered MoS_2 transistors, ACS Nano 7 (6) (2013) 4879–4891.
[14] Q. He, Z. Zeng, Z. Yin, et al., Fabrication of flexible MoS_2 thin-film transistor arrays for practical gas-sensing applications, Small 8 (19) (2012) 2994–2999.
[15] S.S. Gqoba, R. Rodrigues, S.L. Mphahlele, et al., Hierarchical nanoflowers of colloidal ws2 and their potential gas sensing properties for room temperature detection of ammonia, Processes 9 (9) (2021), 9091491.
[16] C. Yang, J. Xie, C. Lou, W. Zheng, X. Liu, J. Zhang, Flexible NO_2 sensors based on WSe_2 nanosheets with bifunctional selectivity and superior sensitivity under UV activation, Sensor. Actuator. B Chem. 333 (2) (2021), 129571.
[17] W. Shi, L. Huo, H. Wang, H. Zhang, J. Yang, P. Wei, Hydrothermal growth and gas sensing property of flower-shaped SnS_2 nanostructures, Nanotechnology 17 (12) (2006) 2918–2924.
[18] S. Veeralingam, P. Sahatiya, S. Badhulika, Low cost, flexible and disposable $SnSe_2$ based photoresponsive ammonia sensor for detection of ammonia in urine samples, Sensor. Actuator. B Chem. 297 (March) (2019), 126725.
[19] C.M. Masemola, N.V. Shumbula, S.S. Gqoba, Z.N. Tetana, N. Nosipho, E.C. Linganiso, Eletrospun NGQDs/PANI/PAN composite fibers for room temperature alcohol sensing, IEEE Conf. (2021) 146–150.
[20] L. Li, R. Lv, J. Wang, et al., Optical nonlinearity of ZrS_2 and applications, Nanomaterials 9 (3) (2019), 9030315.
[21] H.Y. Chen, J. Wang, L. Meng, T. Yang, K. Jiao, Thin-layered MoS_2/polyaniline nanocomposite for highly sensitive electrochemical detection of chloramphenicol, Chin. Chem. Lett. 27 (2) (2016) 231–234.
[22] P. Fadojutimi, Z. Tetana, J. Moma, N. Moloto, S. Gqoba, Colloidal synthesis of zirconium disulphide nanostructures and their stability against oxidation, ChemistrySelect 7 (32) (2022), 202202293.
[23] C.M. Yoon, S. Lee, S.H. Hong, J. Jang, Fabrication of density-controlled graphene oxide-coated mesoporous silica spheres and their electrorheological activity, J. Colloid Interface Sci. 438 (2015) 14–21.
[24] E. Lee, Y.S. Yoon, D.J. Kim, Two-dimensional transition metal dichalcogenides and metal oxide hybrids for gas sensing, ACS Sens. 3 (10) (2018) 2045–2060.
[25] S. Pirsa, Chemiresistive gas sensors based on conducting polymers, Mater Sci Eng Concepts, Methodol Tools 1–3 (2017) 543–574.
[26] I. Fratoddi, I. Venditti, C. Cametti, M.V. Russo, Chemiresistive polyaniline-based gas sensors: a mini review, Sensor. Actuator. B Chem. (220) (2015) 534–548.
[27] B.K. Mutuma, R. Rodrigues, K. Ranganathan, et al., Hollow carbon spheres and a hollow carbon sphere/polyvinylpyrrolidone composite as ammonia sensors, J. Mater. Chem. 5 (6) (2017) 2539–2549.
[28] H. Yan, M. Zhong, Z. Lv, P. Wan, Stretchable electronic sensors of nanocomposite network films for ultrasensitive chemical vapor sensing, Small 13 (41) (2017) 1–8.